A study of wave propagation in varying cross-section waveguides by modal decomposition. Part I. Theory and validation

V. Pagneux
Laboratoire d'Acoustique, URA 1101 CNRS, B.P. 535, Avenue Oliver Messiaen, 72017 Le Mans Cedex, France and Gas Engineering Montrouge, Schlumberger, 50, av. Jean Jaurès, 92542 Montrouge, France

N. Amir and J. Kergomard
Laboratoire d'Acoustique, URA 1101 CNRS, B.P. 535, Avenue Oliver Messiaen, 72017 Le Mans Cedex, France

(Received 9 July 1995; accepted for publication 30 March 1996)

The propagation of acoustic waves in waveguides with variable cross section is considered using multimodal decomposition. The approach adopted is to construct two infinite first-order differential equations for the components of the pressure and the velocity projected over the normal modes. From these an infinite matricial Riccati equation is derived for the impedance matrix. These equations are ordinary differential equations that can be integrated after truncation at a sufficient number of modes and take into account the coupling between modes. The stiffness of the pressure-velocity equations induced by the presence of evanescent modes is avoided by first calculating the impedance matrix along the guide. The method is checked using different examples where the solutions of the plane-wave approximation or the finite element method are known. Results show the method provides simple and accurate means to obtain the acoustic field with correct boundary conditions in a nonuniform guide with no restriction on the flare.

PACS numbers: 43.20.Mv [JEG]

INTRODUCTION

The problem of wave propagation in waveguides of varying cross section has been studied using numerous methods (for a review see Campos[1]). Indeed, while in the case of a uniform guide the analytical solution is well known as a sum of modes, the nonuniform case remains an open problem. For low frequencies and low rates of flare an analysis using the lowest-order mode is often used (see Eisner[2] and Putland[3]). This method assumes a pressure field which is uniform throughout the cross section, or equivalently describes the evolution of the pressure mean value over the cross section when the coupling is neglected. Thus, it is clearly of limited accuracy when the wavelength approaches the transversal dimension of the waveguide. This method also fails at low frequencies if the rate of change in the waveguide cross section is high, because this causes a high degree of mode coupling. In this work we study methods taking higher-order transversal modes into account in cylindrical or Cartesian coordinate systems.

Methods using this type of approach have been previously suggested in the literature. One method was put forth in 1951 by Stevenson,[4] although it was left as an infinite set of equations, with no attempt to solve them, probably due to lack of sufficient computing facilities. Indeed, the problem as posed by Stevenson will later be shown to be nearly impossible to solve. Stevenson's method was based on treating the waveguide as continuous, other methods based on discretizing the geometry have also been proposed.[5,6] These methods have been used successfully to calculate the input impedance and the pressure fields, although they may pose a heavy computational load and may also prove numerically problematic, as will be discussed in detail. Another approach carried out by Kergomard was to take the discrete model to the limit[7] using a matricial formulation, although the resultant pressure equation is, once again, problematic to solve directly.

In this work we address the difficulties mentioned above. Following Kergomard and Stevenson, we project the pressure and axial velocity over the space defined by the local transverse modes at each point along the axis. We then obtain a new equation for the impedance matrix which is numerically workable. We address certain numerical difficulties encountered in solving this equation, and give some practical guidelines on how to choose the relevant parameters necessary to obtain a reasonable solution. We also address the issue of complying with hard boundary conditions using these methods. It has been mentioned in the literature[8] that this is not possible using our approach. We show that by taking the appropriate precautions, the hard boundary conditions can, in fact, be successfully achieved, even if not fulfilled exactly, due to the practical necessity of truncating the infinite series of modes. This and other properties of the solution are demonstrated in a number of examples. We also compare some of our results to those obtained by finite element methods, showing good agreement. The second article[18] (Part II) in this series studies some cases in depth, also comparing theoretical results to experimental results.

Considering the prevalence of purely numerical methods such as finite element or boundary element solutions, we point out that the approach studied here possibly has a number of advantages: These methods enable the calculation of input impedance more directly than previous methods, and

are also convenient for formulating radiating conditions. For a given geometry, once the impedance, truncated at N modes, has been obtained, it is very fast and easy to get the transfer matrix (of dimension $N \times N$) by computing the field with N different sources. From another point of view, an analytic formulation can give a better physical understanding of the problem by analysis of the degree of mode coupling, for instance, and, in some cases, might enable a completely analytical solution of the problem (yet unknown to us). Moreover, an analytic formulation may lead to simple approximations (like the WKB method[4]) useful for solving inverse problems.

The structure of the paper is as follows: in Sec. I we present the basic equations for several methods in matricial form, showing where the various models agree and where they differ. The problem of fulfilling the hard boundary condition is discussed and the analytical precautions necessary to fulfill them are shown. We discuss the problems inherent in solving the pressure equations directly, and present a nonlinear Riccati equation for the impedance matrix, which can be readily solved numerically. In Sec. II we discuss the numerical aspects of the problem. We show how the various parameters must be chosen in order to obtain a reasonable solution, and the practical limitations of the methods suggested. For two common geometries, i.e., axisymmetric and symmetric bidimensional, we explicitly present the associated eigenfunctions and eigenvalues, and the corresponding matrices used in the matricial formulation of the equations. Section III presents a number of examples, comparing the various models proposed, both among themselves and to a finite element solution. These examples are chosen to demonstrate various characteristics of the solution, and to examine its accuracy as far as possible. Finally, the conclusion contains a summary based on the results obtained, pointing out the advantages and drawbacks of the approach used in this paper.

I. DERIVATION OF THE EQUATIONS

We commence by stating the equations on which our discussion will be founded. We then discuss the difficulties encountered using methods found in the literature. Finally, we present the models used here, and show how they address these difficulties.

A. Basic equations

Throughout this paper we will assume adiabatic lossless linear media. We define $\mathbf{v}$ as particle velocity and p as acoustic pressure, with the time dependence $\exp(j\omega t)$ omitted. Without loss of generality, only guides that are symmetrical with respect to the longitudinal axis are considered. This axis corresponds to z coordinate and the transversal coordinate is indifferently called r for both symmetric 2-D and axisymmetric geometries. Defining also the speed of sound as c, and ρ_0 as the density of air, we start from the the equation of mass conservation[9]

$$\operatorname{div}(\mathbf{v}) = -\frac{j\omega}{\rho_0 c^2}\, p, \tag{1}$$

and the equation of momentum conservation

$$j\omega \mathbf{v} = -\frac{1}{\rho_0}\, \boldsymbol{\nabla} p, \tag{2}$$

that yield the three-dimensional wave equation

$$(\Delta + k^2) p = 0, \tag{3}$$

where k is ω/c. We now express the pressure and axial velocity v_z using infinite series

$$p = \sum_i \psi_i(r,z) P_i(z), \tag{4}$$

$$v_z = \frac{1}{S(z)} \sum_i \psi_i(r,z) U_i(z), \tag{5}$$

where P_i and U_i are scalar coefficients, S is the local cross section, and ψ_i are the classical eigenfunctions obeying the transverse Laplacian ($\Delta_\perp$) eigenproblem

$$\Delta_\perp \psi_i = -\alpha_i^2 \psi_i, \tag{6}$$

with the following boundary conditions on the cross-section boundary C:

$$\frac{\partial \psi_i}{\partial r} = 0 \quad \text{on} \quad C, \tag{7}$$

and the orthogonality relation

$$\int \int_S \psi_i \psi_j \, dS = S \, \delta_{ij}, \tag{8}$$

where S is the cross section and r is the transverse ordinate. The eigenvalues of these eigenfunctions are given, respectively, in an axisymmetric and in a symmetric bidimensional geometry by

$$\alpha_n(z) = \frac{\gamma_n}{R} \quad \text{and} \quad \alpha_n(z) = \frac{n\pi}{h}, \tag{9}$$

where the γ_n are the successive zeros of the Bessel function of order one, R is the waveguide radius (axisymmetric geometry), and h is the waveguide half-height (symmetric bidimensional geometry). Note that the eigenfunctions are not orthonormal, as they often are in the literature;[4] their inner product is always S. This can often prove to be more convenient, as described in Ref. 10. Following the matricial terminology we will write the above modal decompositions (4) and (5) as

$$p = {}^t\boldsymbol{\psi}\mathbf{P}, \tag{10}$$

$$v_z = \frac{1}{S}\, {}^t\boldsymbol{\psi}\mathbf{U}, \tag{11}$$

where $\mathbf{P}$, $\mathbf{U}$, and $\boldsymbol{\psi}$ are column vectors.

Considering now a waveguide discontinuity (see Fig. 1), we can express the pressure and velocity on one side of the discontinuity, when they are known on the other side, by the two equations obtained by projection on the eigenfunctions.[10] Indeed, since $p_1 = p_2$ and $v_{z1} = v_{z2}$ and S_1 and $v_{z2} = 0$ on $S_2 - S_1$, projections yield

$$\mathbf{P}_1 = F\mathbf{P}_2, \tag{12}$$

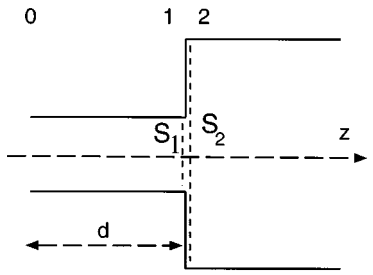

FIG. 1. Geometry of a typical discontinuity.

$$\mathbf{U}_2 = {}^tF\mathbf{U}_1, \tag{13}$$

where the matrix F is defined by

$$F_{ij} = \frac{1}{S_1}\int\int_{S_1} \psi_{1i}\psi_{2j}\, dS. \tag{14}$$

Note that this formulation corresponds to the Mixed Method as defined by Vassallo,[11] where the correct boundary condition, $v_{z2}=0$, is achieved on the surface S_2-S_1. The latter also defines a Unilateral Method which is different and does not provide any boundary condition on the vertical wall of the discontinuity: Matching only the velocity on S_1 gives

$$\frac{1}{S_1}\mathbf{U}_1 = F\,\frac{1}{S_2}\mathbf{U}_2. \tag{15}$$

Note that with (13) we can thus write

$$\left({}^tFF - \frac{S_2}{S_1}\right)\mathbf{U}_2 = 0. \tag{16}$$

It is impossible to conclude from (16) that ${}^tFF = S_2/S_1 I$ (where I is the identity matrix) because $\mathbf{U}_2$ is not a free vector; it has to be such that $v_{z2}=0$ on the surface S_2-S_1. Hence, we can only say that S_2/S_1 is an eigenvalue of the symmetric matrix $A={}^tFF$ associated to the eigenvector $\mathbf{U}_2$. A straightforward proof is to see that $A_{00}=1\neq S_2/S_1$. On the other hand, from (13) and (15) we obtain $F{}^tF = S_2/S_1 I$, which is a correct relation since $\mathbf{U}_1$ is free.

We also note that the first element of $\mathbf{U}$ is actually the volume velocity, since the higher-order modes have no net contribution to this value. In the following we will loosely refer to the entire vector $\mathbf{U}$ as the volume velocity.

B. The models used

In a varying cross-section waveguide we will present three formulations for finding the coefficient vectors $\mathbf{P}$ and $\mathbf{U}$ above, inspired mainly by Refs. 4, 6, and 7. The two main problems with these existing formulations are the direct solution of the pressure-velocity equation and dealing with hard boundary conditions.

Let us first consider a typical physical case of a finite waveguide; the radiation impedance is known at the right and the source is known at the left. If we wish to solve the differential equation for only the pressure in the waveguide, we will not in fact have the boundary conditions necessary for its solution. For instance, imposing a boundary condition of both pressure and the derivative of the pressure (which is equivalent to velocity) at the right, and then integrating down to the source leaves no degree of freedom at the source. On the other hand, imposing both boundary conditions at the source implies *a priori* knowledge of the impedance at the source, and leaves no degree of freedom for choosing the radiation impedance. The best way to solve the problem is to find an equation for the impedance (which will be a matrix in our formulation), imposing the known radiation impedance at the right as a boundary condition. This type of impedance matrix was calculated by Zorumski[12] for radiation from an opening in an infinite baffle, and used by Roure.[6] The equation can then be integrated down to the source. The source will usually be characterized as a known velocity or pressure, so once the impedance is found the missing value (pressure or velocity) can be calculated. The pressure or velocity field throughout the waveguide can then be calculated, as we show later. Thus, physically, we must first solve the impedance problem to model a realistic situation.

The method stated above solves another problem encountered in the pressure equation, which is that it is often found to be stiff.[8] Thus, it can be quite difficult to solve, even when the boundary conditions are supplied. Finding the impedance equation is a method commonly used for overcoming this problem, as demonstrated in Ref. 13 for a scalar equation. An alternative would be the use of a shooting method that is, nevertheless, not very convenient in a multimodal approach.

The second major problem encountered with the modal decomposition approach is that of complying with the hard boundary conditions along the waveguide. At the wall this boundary condition implies

$$\frac{\partial p}{\partial n} = \frac{\partial p}{\partial r} - R'(z)\,\frac{\partial p}{\partial z} = 0, \tag{17}$$

where $\partial/\partial n$ is the normal derivative and R' the derivative of the radius of the guide. When applying this boundary condition to the series representation of the pressure we obtain $(\partial/\partial n)\Sigma_i \psi_i P_i = 0$. Applying (17) to the solution of (3) is not trivial because the series cannot be, *a priori, derived term by term everywhere*, i.e., the derivative of the series is not always the series of the derivatives. It is a key point since a major criticism (see Ref. 14) to the projection on the transverse modes is that, for each mode that has vertical gradient at the wall ($\partial p/\partial r = 0$), the series representation cannot achieve the right boundary condition ($\partial p/\partial n = 0$) when $R'\neq 0$.

An example of a similar case is encountered when projecting a cosine function $t\rightarrow\cos(at)$, defined on the interval $[-1,1]$, on the Fourier basis $t\rightarrow\cos(n\pi t)$. There, as well, the series converges but cannot be derived term-by-term everywhere. Indeed, every basic function has a zero derivative for $t=1$ but the corresponding value for the cosine function $t\rightarrow\cos(at)$ is $-a\sin(a)$ which, in general, is not zero. At $t=\pm 1$ the series of the derivatives is not the derivative of the series, but that does not mean that the series representation of the function is not valid (Ref. 19).

Often in the literature the true boundary condition is not fulfilled, but a simpler one is used where the velocity is set to zero perpendicular to the axis instead of to the walls.[14] On

the other hand, applying (17) carefully through an integral method (see Appendix B) enables us to fulfill the true boundary conditions. Practical limitations dictate usage of a truncated series, yet this will still give good results, as shown in Sec. III.

Keeping the above points in mind, we now present the models used in this work.

1. The discrete model

This model treats the waveguide as a series of regularly shaped segments. For example, an axisymmetric waveguide is treated as a series of short cylinders, whose radii vary in a manner approximating the shape of the waveguide. A full treatment of this model has been presented by Alfredson,[5] Roure,[6] and Kergomard *et al.*[15] In the following we will call it the DS (discrete segment) method. Although the equations in this model are algebraic, as opposed to differential equations for the continuous models, the difficulties mentioned above also exist. To resolve them Roure presents equations for an impedance matrix instead of pressure or velocity.

We present here a summary of Roure's method, adapted to our notation. The first step is to define a generalized impedance, which is a matrix Z fulfilling:

$$\mathbf{P}=Z\mathbf{U}. \tag{18}$$

Looking at Fig. 1, we wish to obtain a relationship between the impedance at the right of the junction $Z^{(2)}$, which is the input impedance to the right waveguide segment, and $Z^{(0)}$, which is the input impedance of the left segment. In the one-mode (plane-wave) model, $Z^{(2)}$ and $Z^{(1)}$ would be equal due to the fact that the plane-wave volume velocity and pressure are equal at either side of the junction. In our case, the continuity of pressure and volume velocity are governed by (12) and (13). Substituting (18) into (13) we obtain

$$Z^{(1)}\mathbf{U}^{(1)}=FZ^{(2)}\mathbf{U}^{(2)}, \quad {}^{t}F\mathbf{U}^{(1)}=\mathbf{U}^{(2)}. \tag{19}$$

From (19) we then find, since $\mathbf{U}^{(1)}$ is an arbitrary vector,

$$Z^{(1)}=FZ^{(2)}{}^{t}F. \tag{20}$$

To find the relationship between $Z^{(1)}$ and $Z^{(0)}$ we examine the equations governing the propagation of pressure and velocity from one side of a waveguide segment to the other. Since the waveguide cross section is constant over this segment, the propagation of these is determined simply by the characteristic impedance for each mode, with no coupling. Defining the diagonal matrices D_1, D_2, and N as follows (index i refers to the ith element of the diagonal): $D_1=\cos(k_i,d)$, $D_2=j\sin(k_i d)$, and $Z_c=k\rho c/k_i S$, where $k_i^2=k^2-\alpha_i^2$. It can be easily shown that

$$\mathbf{P}^{(0)}=D_1\mathbf{P}^{(1)}+D_2Z_c\mathbf{U}^{(1)}, \tag{21}$$

$$\mathbf{U}^{(0)}=D_2Z_c^{-1}\mathbf{P}^{(1)}+D_1\mathbf{U}^{(1)}. \tag{22}$$

Once more, substituting (18) into (21), we can obtain

$$Z^{(0)}=(D_1Z^{(1)}+D_2Z_c)(D_2Z_c^{-1}Z^{(1)}+D_1)^{-1}. \tag{23}$$

Although this equation is algebraic, applying it to a real case causes divergence resembling the divergence of a stiff differential equation. This is because the elements of D_1 and D_2 contain very large numbers for the evanescent modes, which cause expontential divergence of the computation due to the finite precision of the computer. Another form which is more useful is suggested by Roure; defining $D_3=\tan(k_i d)$, we have

$$Z^{(0)}=D_3^{-1}Z_c-D_2^{-1}[Z^{(1)}+D_3^{-1}Z_c]^{-1}D_2^{-1}. \tag{24}$$

If we are now given a discretized waveguide and its radiation impedance, we can propagate this impedance down to the source, alternately using (20) and (24).

Propagating the pressure or volume velocity down the waveguide is now possible. We can use either (21), (22), or equivalent equations obtained by substituting (18) into (22), such as

$$\mathbf{U}^{(1)}=(-D_2Z_c^{-1}(Z^{(0)}-Z_c)+e^{-jk_i d})\mathbf{U}^{(0)}. \tag{25}$$

In Sec. II we will discuss the numerical problems encountered when implementing this method.

The question of fulfilling the correct boundary conditions arises here once more. At first glance it may seem that the velocity is zero in a direction perpendicular to the axis, instead of the waveguide wall. Yet, in fact, at each junction of two cylinders we also impose that the velocity is zero at the surface S_2-S_1 (see Fig. 1) in the direction parallel to the waveguide axis. We can argue that as the lengths of the cylindrical segments tend to zero, the equivalent of these two becomes zero velocity perpendicular to the waveguide wall. A more rigorous analysis in Sec. I B 3 strengthens this argument.

2. The discrete model carried to the limit

The formulation described in Sec. I B 1 can be carried to the limit of infinitesimal segment length, as shown by Ref. 7; we will call it the IDS (infinitesimal discrete segment) method. Taking the limit of successive discontinuities [see Eqs. (12) and (13)] and straight guides (21) and (22) results in two first-order differential equations for velocity and pressure. First, we note that the derivatives in a straight section are $\mathbf{P}'=-j(\omega\rho/S)\mathbf{U}$ and $\mathbf{U}'=-j(S/\omega\rho)K\mathbf{P}$, where the matrix K is diagonal and is defined by $K_{ij}=(k^2-\alpha_i^2)\delta_{ij}$. We have a correction to Ref. 7 for the proof of the derivative part due to the infinitesimal discontinuity which comes from the care that has to be taken when using the first-order expansion $F=I-\epsilon Q$ (where $\epsilon=S_2-S_1/S_1\to 0$, see Appendix A). Eventually, the matricial horn first-order differential equations are

$$\mathbf{P}'=\frac{S'}{S}\,Q\mathbf{P}-j\,\frac{\omega\rho}{S}\,\mathbf{U}, \tag{26}$$

$$\mathbf{U}'=-j\,\frac{S}{\omega\rho}\,K\mathbf{P}-\frac{S'}{S}\,{}^{t}Q\mathbf{U}, \tag{27}$$

where the matrix Q is constant. In axisymmetric geometry it is zero on the diagonal, with the rest of its elements being

$$Q_{ij}=\frac{\gamma_j^2}{\gamma_j^2-\gamma_i^2}. \tag{28}$$

By simply combining these two first-order differential equations, it *seems* possible to obtain a second-order differential equation for the pressure (note a minor correction to Ref. 7):

$$\mathbf{P}''+\frac{S'}{S}\,(1-Q+{}^tQ)\mathbf{P}'+K\mathbf{P}-\left(\frac{S''}{S}\,Q+\frac{S'^2}{S^2}\,{}^tQQ\right)\mathbf{P}=0. \tag{29}$$

It should be kept in mind that to obtain (29) one has to derive infinite series term-by-term. This will be discussed further in Sec. I C.

Due to the difficulties mentioned above that are inherent in directly solving this type of equation, we will instead use an equation for the impedance matrix Z defined by Roure, as presented in Sec. I B 1 [Eq. (18)]; then we can obtain a Riccati equation for Z.

First, at a discontinuity, using (20) and the development for the matrix $F=I-\epsilon Q$,

$$Z^{(1)}=Z^{(2)}-\epsilon(QZ^{(2)}+Z^{(2)t}Q); \tag{30}$$

thus, by taking the limit when $\epsilon\to 0$, the part due to the varying cross section is

$$Z'=\frac{S'}{S}\,(QZ+Z^tQ), \tag{31}$$

and adding the part due to propagation in the cylinder the entire equation that governs Z is

$$Z'=-j\,\frac{\omega\rho}{S}+j\,\frac{S}{\omega\rho}\,ZKZ+\frac{S'}{S}\,(QZ+Z^tQ). \tag{32}$$

The same equation is obtained if we begin with the *a priori* illicit derivation of (18), $P'=Z'U+ZU'$; we then substitute U' from (26), U from (18), and retain the coefficients of U to obtain Eq. (32) (see Ref. 16).

Equation (32) can be integrated from the free end of the waveguide down to the source, usually without encountering numerical difficulties. The velocity can then be calculated as follows: we once again substitute (18) in (26) to obtain

$$\mathbf{U}'=\left(-j\,\frac{S}{k}\,Z_c^{-1}KZ-\frac{S'}{S}\,{}^tQ\right)\mathbf{U}. \tag{33}$$

Z should be stocked at each point when integrating (32), and then Eq. (33) can be integrated from the source to the radiating end of the waveguide, giving $\mathbf{U}$ at each point. The pressure can afterwards be calculated from (18), once $\mathbf{U}$ and Z are known, or else an equation analogous to (33) can be derived, using the admittance matrix (which is defined by $\mathbf{U}=Y\mathbf{P}$). This whole procedure is performed to avoid the divergence due to evanescent modes. (A continuous equation can also be found for the reflection matrix, but it presents a singular coefficient at the cut-on frequencies of the transversal modes.)

The argument presented in Sec. I B 1 for fulfillment of the true hard boundary conditions is also valid here. It will be verified further using Stevenson's approach to imposing the boundary conditions, described in Sec. I B 3.

3. The purely continuous model

In a paper appearing in 1951,[4] Stevenson presented an infinite set of second-order differential equations for the velocity potential in nonuniform waveguides. This set of equations is obtained by applying the modal decomposition directly to wave equation (3); in subsequent analysis, application of boundary condition (17) is performed rigorously. We will call this method the cw (continuous waveguide) method. Stevenson uses a slightly different (orthornormal) definition of the eigenfunctions v_n:

$$v_n=\psi_n/\sqrt{S}. \tag{34}$$

Defining the velocity potential as $\phi=\Sigma_n\phi_n v_n(z)$, Stevenson obtains the set of equations

$$\phi_n''+\sum_m X_{nm}\phi_m'+\sum_m Y_{nm}\phi_m=0, \tag{35}$$

where

$$\begin{aligned} X_{nm}&=A_{nm}-A_{mn},\\ Y_{nm}&=(k^2-\beta_n^2)\,\delta_{nm}+C_{nm}+D_{nm}, \end{aligned} \tag{36}$$

and

$$\begin{aligned} A_{mn}&=\int_A v_m\,\frac{\partial v_n}{\partial z}\,dS,\quad B_{mn}=\int_C \tan\,\theta v_m v_n\,ds,\\ C_{mn}&=\int_A v_m\,\frac{\partial^2 v_n}{\partial z^2}\,dS,\quad D_{mn}=\int_C \tan\,\theta v_m\,\frac{\partial v_n}{\partial z}\,ds, \end{aligned} \tag{37}$$

where θ is the angle of the flare at this abscissa and A and C, respectively, denote surface and curve integrals. Stevenson did not attempt to solve these equations numerically, although they are indeed stiff due to the evanescent modes, and thus quite difficult to solve.

a. Applying Stevenson's method to the first-order differential equations. In view of Stevenson's treatment of the boundary conditions, it would be interesting to use the methods he applied to wave equation (3), for instance, on the two first-order differential equations (1) and (2) in the case of axisymmetric geometry. Multiplying each of them by ψ_n and integrating over the cross section S gives us for each component n

$$\begin{aligned} (SP_n)'=&-j\omega\rho U_n+\sum_n\left(\int\int_S \psi_m\,\frac{\partial\psi_n}{\partial z}\,dS\right)P_m\\ &+\sum_m\left(\oint_C \psi_m\psi_n R'(z)\,dC\right)P_m, \end{aligned} \tag{38}$$

$$\begin{aligned} U_n'=&-\frac{jS}{\omega\rho}\,(k^2-\alpha_n^2)P_n\\ &+\frac{1}{S}\sum_m\left(\int\int_S \psi_m\,\frac{\partial\omega_n}{\partial z}\,dS\right)U_m \end{aligned} \tag{39}$$

using the identities presented in Appendix B. Examining the expression for the surface integrals in Eqs. (38) and (39), we can obtain the following relationship involving the Q matrix:

$$\int \int_S \psi_m \frac{\partial \psi_n}{\partial z}\, dS = -S' \frac{\gamma_n^2}{\gamma_n^2 - \gamma_m^2} = -S' Q_{mn}. \tag{40}$$

On the other hand, using the fact that $\psi_n(R)=1$ in the axisymmetric case, one gets $\oint_C \psi_m \psi_n R'(z)\, dC = 2\pi R R' = S' \Theta_{mn}$, where $\Theta_{ij}=1$. Substituting (40) into (38) we obtain

$$\mathbf{P}' = -j \frac{\omega \rho}{S} \mathbf{U} + \frac{S'}{S} (\Theta - {}^tQ - I)\mathbf{P}, \tag{41}$$

$$\mathbf{U}' = -\frac{jS}{\omega \rho} K\mathbf{P} - \frac{S'}{S} {}^tQ\mathbf{U}. \tag{42}$$

We see in fact that (26) and (27) and (41) and (42) are identical since it is easy to prove that

$$Q + {}^tQ + I = \Theta. \tag{43}$$

In other words, the IDS and cw methods give the same result when analyzed to yield ordinary first-order differential equations.

These comparisons bring to light a few interesting facts, summarized here:

(i) The IDS and cw methods give equivalent coupled first-order differential equations.

(ii) Since the CW method complies with the hard boundary conditions, so does IDS. Furthermore, since the IDS method is simply DS carried to the limit, we can expect the DS method to approximate the true hard boundary conditions, depending on the discretization. In either case, we do not have to require that the cross section change gradually in comparison to wavelength.

(iii) Extending the first-order differential equations obtained using the IDS and cw methods to obtain a second-order pressure differential equation, as one in Ref. 7, does not give an identical equation to that obtained by Stevenson. This is discussed further in the Sec. IC.

C. Second-order differential equations

In view of the above discussions regarding the first-order matricial differential equations for **P**, **U**, and Z, it is interesting to put them into perspective with respect to other treatments of the problem at second order.[4,7,8] In fact, the purpose of this section is mainly to show the problems inherent in a second-order analysis rather than to solve them. This stems from the fact that the first-order analysis presented above could be followed through rigorously [i.e., without deriving series term-by-term; see discussion on Eq. (17)], giving consistent results, whereas the second-order analysis proved to be inconclusive.

First of all, it is troubling to observe that a number of different second-order differential equations can be obtained using the same basic methods. The first is Eq. (29), obtained directly from the matricial representation of the first-order differential equations. In other words, it is obtained by first projecting the first-order equations and then combining them. This involves derivation of infinite sums term-by-term, and is therefore mathematically suspect. When degenerated to one single mode we obtain the well-known matched-plane wave (MPW) equation (often called the horn or Webster equation, actually due to Lagrange, see Ref. 2 and Appendix D). In this paper we will use the MPW equation; this is no promise of the validity of this equation.

On the other hand, another approach would be to follow Stevenson, by projecting the Helmhotz equation over the eigenfunctions. This results in a different equation, as follows:

$$\mathbf{P}'' + \frac{S'}{S}(1 + Q - {}^tQ)\mathbf{P}' + (k^2 - A)\mathbf{P} - \left(\frac{S''}{S} ({}^tQ - Q) + \frac{1}{S} T(z) \right)\mathbf{P} = 0, \tag{44}$$

where $T(z)$ is defined by $\int\int \psi''^t \psi \mathbf{P}\, dS = T\mathbf{P}$ (see Appendix H). Not only is this equation different from the previous one, it is also slightly different from Stevenson's own result, when translated to the appropriate notation. Both of these degenerate to the MPW equation when higher-order modes are ignored, and yet again both contain derivations of infinite series term-by-term; evidently Stevenson was not aware of this fact, since it is not mentioned in his paper.

A more rigorous procedure, completely avoiding derivations of infinite sums, results in the third equation (45), as presented in Appendix C, which is once again different from the previous two second-order pressure differential equations:

$$\mathbf{P}'' + \frac{S'}{S}[(1 - R'^2)\Theta - 2Q]\mathbf{P}' + (k^2 - A)\mathbf{P} + \left(\frac{S''}{S} (I - \Theta) + \left(\frac{S'}{S} \right)^2 [(1 + R'^2)\Theta Q - 2{}^tQQ] - \frac{1}{S} T(z) \right)\mathbf{P} = 0. \tag{45}$$

This equation, which is the correct one, does not degenerate into the MPW equation when higher-order modes are ignored but into $p'' + S'/S(1 - R'^2)p' + k^2 p = 0$, which is once more unexpected.

Having now obtained three different second-order pressure differential equations, it remains to try to solve them. As mentioned before, this is also a problem, due to the fact that it is difficult to pose an appropriate boundary condition; furthermore, the equations are stiff and therefore numerically very unwieldy. One possibility would be to obtain a Riccati equation directly from the pressure equation, defining the matrix H by

$$P = -\frac{S}{j\omega \rho} HP'. \tag{46}$$

If we derive (46) and substitute from (29) for P'', and from (46) for P, retaining the coefficients for P' gives the Riccati equation for H:

$$H' = -\frac{j\omega \rho}{S} + \frac{jS}{\omega \rho} H\left(\frac{S''}{S} Q + \frac{S'^2}{S^2} Q^t Q \right) H + H(1 - Q + Q^t) - \frac{S'}{S} H. \tag{47}$$

The problem with this procedure is that, once more, in deriving (46) we are deriving an infinite series term-by-term, and thus the results are suspect as discussed for Eq. (17).

Nevertheless, solving (47) gave results very similar to solving (32), as shown in Sec. III. Carrying out the same procedure for (44) gave generally similar results, although they were much less self-consistent in that the energy flux along the guide fluctuated by about 40%, thereby showing them to be false.

In conclusion, we have shown that the second-order differential equations are difficult to deal with, and furthermore do not seem in any way to improve the results obtained solely using first-order differential equations. In general, it seems that any results obtained from these equations must be treated with caution. Eventually, to decide which one is correct could be possible by applying our method in variable cross waveguides where the problem is exactly solvable. But in these cases (a cone, for example) the radiation conditions are not convenient in terms of impedance matrix.

D. Energy flux

One way to examine the accuracy of the pressure and velocity calculations is to compute the energy flux along the waveguide. In the case of lossless propagation, this value should remain constant. In this section we will examine this point analytically, and in Sec. III it will be calculated numerically for the examples presented there. Using the matricial notation, the energy flux is simply

$$W=\tfrac{1}{2}\,\mathrm{Re}\{{}^t\mathbf{P}\mathbf{U}^*\}, \tag{48}$$

where (*) denotes complex conjugate. In the following we analyze this value for each of the models presented in this section.

In the DS method we must examine energy flux conservation for two separate cases: propagation across a waveguide segment and propagation across a waveguide discontinuity. The first case is trivial since we are dealing throughout with a lossless uniform waveguide; in the second we show that the energy flux on one side of the discontinuity, $(1/2)\mathrm{Re}\{{}^t\mathbf{P}_2\mathbf{U}_2^*\}$, is equal to that on the other side, $(1/2)\mathrm{Re}\{{}^t\mathbf{P}_1\mathbf{U}_1^*\}$. From (13) we have $\mathbf{U}_2={}^tF\mathbf{U}_1$, and thus the energy flux on the two sides of the discontinuity is shown to be equal:

$$\mathrm{Re}\{{}^t\mathbf{P}_2\mathbf{U}_2^*\}=\mathrm{Re}\{{}^t\mathbf{P}_2^tF\mathbf{U}_1^*\}=\mathrm{Re}\{{}^t\mathbf{P}_1\mathbf{U}_1^*\}. \tag{49}$$

In the IDS model, the $\mathbf{P}$ and $\mathbf{U}$ vectors are continuous functions of z. Therefore, in order to demonstrate that the energy flux is constant, we can show that its derivative is zero. Deriving (48), and substituting (26) and (27), we obtain, after some algebra,

$$\begin{aligned}2W'&=\mathrm{Re}\{{}^t\mathbf{P}'\mathbf{U}^*+{}^t\mathbf{P}^t\mathbf{U}^{*\prime}\}\\&=\cdots=\mathrm{Re}\left\{\frac{-j\omega\rho}{S}\,{}^t\mathbf{U}\mathbf{U}^*+\frac{jS}{\rho\omega}\,{}^t\mathbf{P}K\mathbf{P}^*\right\}=0,\end{aligned} \tag{50}$$

as expected.

II. NUMERICAL CONSIDERATIONS

The various equations posed in the previous section will not be amenable in general to analytic solution. They will therefore usually have to be resolved numerically. In this section we discuss the problems encountered when implementing a numerical solution, considering in particular two specific types of geometries: the axisymmetric geometry and the symmetric bidimensional geometry. We commence by presenting the formulation of the F and Q matrices for these geometries.

A. Symmetric bidimensional geometry

A typical junction in this kind of geometry is depicted in Fig. 1. The waveguides are infinite in the x direction, symmetrical around the z axis, and the height varies in the y direction. The eigenfunctions fulfilling Eqs. (6)–(8) are, in this case,

$$\psi_n=\begin{cases}1, & n=0,\\ \sqrt{2}\,\cos\dfrac{m\pi y}{h}, & m\neq 0.\end{cases} \tag{51}$$

The matrix F at a junction between two waveguides is given by (14). In this particular case, for two waveguides whose half-heights are h_1 and h_2, respectively, we have,

$$F_{nm}=\begin{cases}1, & m=n=0\\ \sqrt{2}\ \mathrm{sinc}\,(m\pi a), & n=0,\ m>0,\\ 1, & n_{h_1}=m/h_2,\\ 2(-1)^n\dfrac{(ma)^2}{(ma)^2-(n)^2}\,\mathrm{sinc}\,(m\pi a), & \text{otherwise,}\end{cases} \tag{52}$$

with $a=h_1/h_2$ and $\mathrm{sinc}(x)=\sin(x)/x$, $\mathrm{sinc}(0)=1$. Considering the asymptotic case where $\epsilon=(h_2-h_1)/h_1$ tends to zero, we obtain

$$F\approx I-\epsilon Q, \tag{53}$$

where I is the identity matrix and Q is given by

$$Q_{nm}=\begin{cases}1/2, & m=n,\\ 2(-1)^{m+n}\dfrac{m^2}{m^2-n^2}, & \text{otherwise.}\end{cases} \tag{54}$$

B. Axisymmetric geometry

A junction in this geometry is shown in Fig. 1. The axial coordinate is z and r is perpendicular to z. R_1 and S_1 are the radius and cross section of the first waveguide, and R_2 and S_2 are the radius and cross section of the second one. The eigenfunctions are

$$\psi_n(r)=\frac{J_0(\gamma_n r/R)}{J_0(\gamma_n)}. \tag{55}$$

Then the matrix F is $(m\neq n)$:

$$F_{nm}=\frac{2x\gamma_m J_1(x\gamma_m)}{(x^2\gamma_m^2-\gamma_n^2)J_0(\gamma_m)}, \tag{56}$$

where $x=R_1/R_2$ and $F_{00}=1$. When x tends to unity, or $\epsilon=(S_2-S_1)/S_1$ tends to zero, F can be expressed once more as in (53), where Q is, in this case,

$$Q_{nm}=\begin{cases}0, & m=n,\\ \dfrac{\gamma_m^2}{\gamma_m^2-\gamma_n^2}, & \text{otherwise.}\end{cases} \tag{57}$$

C. Numerical solutions and various accompanying problems

In general, Eqs. (32) and (33) cannot be solved analytically. The methods used here for solving these equations were third- or fourth-order Runge–Kutta algorithms, as found in Ref. 13. The use of an adaptive step size was found to be imperative for Eq. (32), using the sum of the components of the Z matrix as a rough ''magnitude'' for the error calculations. As described below, an adaptive stepsize could not be used for integrating (33), although with tuning of the fixed step size this proved to be accurate enough.

Implementing the Runge–Kutta algorithms brought to light a number of pitfalls and practical problems. These are summarized here, along with possible methods to avoid them.

1. Selecting the number of modes

Since the numerical solution requires truncating the infinite series of modes so that Q is a finite matrix, and the pressure and velocity are represented by finite series, the first problem is that of choosing the number of modes to conserve. This will usually depend on the frequency and geometry of the waveguide in question. It cannot be stated categorically that all the propagating modes plus four or five evanescent modes are sufficient; in Sec. II C 2 we present an example requiring approximately 17 evanescent modes to achieve a result in agreement with that obtained by finite elements, although there is only one propagating mode. In general, the larger the degree of flare in the waveguide, the larger the coupling between the modes, requiring a large number of modes. The best method to determine the number of modes is to perform the computation using successively more modes, until the solution remains unchanged.

2. Divergence of the Riccati equation

Another problem that may occur is that the solution of the Riccati equation may in some cases diverge. Consider a simple case of one mode only, with no losses, frictional or radiative, such as a closed straight tube. The impedance calculated along the waveguide in such a system is proportional to $\tan(kz)$ and will have peaks of infinite height, meaning Z will diverge. The same holds for the multimodal case. A nondiverging solution requires at least one mechanism of loss, either by radiation or lossy propagation. The former is determined by the boundary condition for the impedance; for instance, using a boundary condition equal to the characteristic impedance of an infinite tube assumes a ''matched termination,'' implying a large degree of radiation loss. In most cases the boundary condition will not in fact be totally reflecting, but if it is then a small negative real part must be added to the wave numbers of the propagating modes to ensure convergence (see Ref. 17).

A related problem may crop up when computing the pressure or velocity. For instance, calculating the velocity along the waveguide entails integrating (33) or (46), which in turn require the values of Z along the waveguide. Note that these equations are integrated from the source to the free end of the waveguide, after the impedance has been integrated in the opposite direction. Thus, the pressure and impedance cannot be integrated simultaneously. This means the values of Z along the waveguide must either be stored during the initial integration or recomputed along with the pressure integration. Implementing the former is straightforward, yet may cause memory problems. Assuming, for example, 1000 integration points and 15 modes, storing the complex impedance matrix at each point requires approximately 3.5 Mb of memory. As an alternative, we attempted to reintegrate the Riccati equation for the impedance in the reverse sense, from the source to the free end of the waveguide, using the previously computed input impedance as the boundary condition. This integration proved to be inaccurate, either diverging or giving large errors for the impedances of the evanescent modes. This behavior may be simply understood; let us model the impedance equation by $Z'=-j(1-(Z/Z_c)^2)$. Then the characteristic impedance towards the right is $Z_c=k/(Sk_n)$. If Z_c is pertubated by an infinitely small quantity ζ (such as a numerical error), $Z=Z_c+\zeta$, and the evolution of ζ is $\zeta'=2j/Z_c[\zeta+\zeta^2/(2Z_c)]=\lambda\zeta+O(|\zeta|^2)$. Thus, if the linear growth $\mathrm{Re}(\lambda)$ is positive, the perturbation ζ will first grow exponentially and saturate due to the second-order term. It is what we observe when we try to integrate upwards a characteristic impedance $Z_{mn}=k/(Sk_n)\delta_{mn}$; the propagating modes keep their correct value (real positive) but the vanishing ones that should be imaginary positive become imaginary negative because of the numerical instability described above. In fact, once more, we see evidence of the hazardous nature of the vanishing modes.

3. Implementing the DS method

Implementing this method entails solving a series of algebraic equations instead of a differential equation. Both an advantage and a drawback of this method is that it uses the true (but truncated) F matrix instead of its linear approximation. Although this may be more accurate, the load of recalculating F for every scattering junction may prove to be prohibitive. One method to overcome this is to partition the waveguide in such a way that the area ratio between two successive segments is always the same, thus enabling use of the same F matrix throughout. This is feasible, although it also involves a certain amount of computation.

Another problem encountered when implementing this method is that if the difference in cross section between successive segments is too large, the resulting impedance calculated along the waveguide contains a large amount of ripple, as opposed to the smooth results obtained using the Riccati equation proposed here.

III. EXAMPLES

In this section we show how the methods above can be applied to two examples, demonstrating various properties of the solutions.

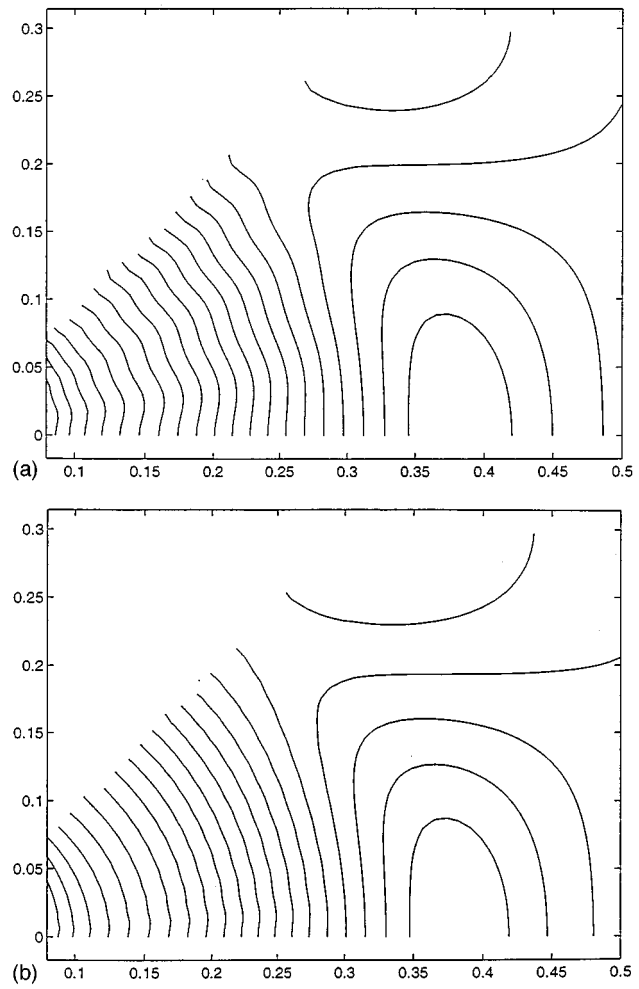

FIG. 2. Isobar surfaces in a cone terminated by an infinite pipe, using (a) seven transverse modes, (b) 17 transverse modes. The ripple in (a) is nearly absent in (b).

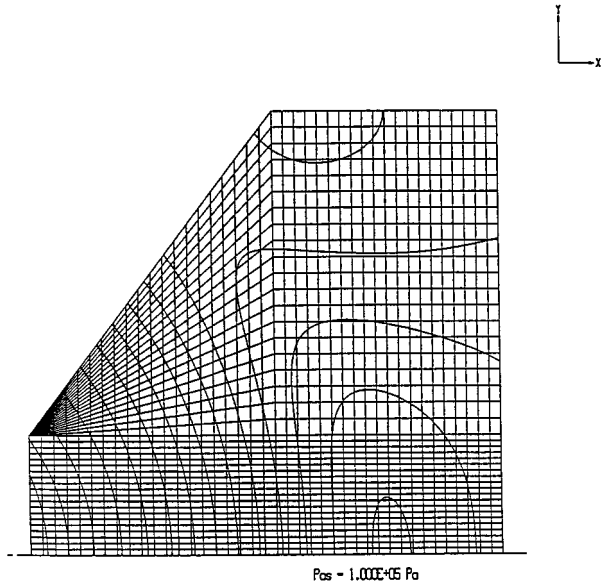

FIG. 3. Isobar surfaces in a cone terminated by an infinite pipe, calculated using the ATTILA finite element program.

We will first consider the case of a truncated cone, with an apex half-angle of 45°, terminated by an infinite pipe. The purpose of this final pipe is to supply a very simple radiation impedance matrix, equal to the diagonal characteristic impedance in the pipe. We expect the equiphase surfaces in this waveguide to resemble spherical caps in the conical section. This should be true regardless of the frequency in question. Thus, we will examine a case where all of the higher-order modes in the waveguide are in cutoff; any deviation from planar wave propagation will be solely due to mode coupling. In our case the initial radius will be 0.08 m, the terminating radius will be 0.3 m, and the frequency of analysis will be 600 Hz. Note that at this frequency all of the modes above the zeroth-order mode are evanescent; the excitation will be a planar piston at the small end of the waveguide, and thus any excitation of higher-order modes is solely due to mode coupling.

In Fig. 2 we see the resulting equipressure contours for analyses carried out with 7 and 17 modes, using the Riccati equation (32), and then computing the pressure as described in Sec. I B 2. We observe there is a fair amount of ripple in the former; this stems from the fact that it takes more than the first seven eigenfunctions to achieve a good approximation to a spherical shape. In the second case, using 17 modes, the ripple is nearly absent. This exemplifies how choosing the number of modes is influenced by the geometry, so in some cases many evanescent modes are necessary. Observing the analysis using 17 modes, we also see that the boundary conditions are approximated better, since the contours are almost perfectly perpendicular to the boundaries, implying a zero pressure gradient there. Near the source the contours tend to be spherical, as expected.

In Fig. 3 we present results of the same calculation, using a finite element analysis (ATTILA). The results thus obtained are very close to those obtained by the modal decomposition. Furthermore, with our method, calculating the energy flux along the waveguide gave a maximum deviation of 0.001% between the minimum and maximum values. This compares very favorably with the results of Ref. 8, which were in the vicinity of 10%. Solving Stevenson's pressure equation by the substitution described in Sec. I C gave quite a large deviation of 40%.

Another problem of interest is the circular cross-section exponential horn. In this case, we know the analytical solution of the matched plane-wave approximation equation (which we will call MPW, but is often also called the ''Webster equation,'' actually due to Lagrange, see Ref. 2 and Appendix E). It yields, for instance, that for the infinite case there is a cutoff frequency below which there is no wave that can propagate down the horn. For the finite case, although there may be some kind of tunneling for the plane wave, the cutoff is still efficient. Thus, it is possible to compare it to our results. The chosen geometry is an exponential of length L terminated by an infinite straight duct of radius R_f and excited at its throat by a plane piston of radius R_0. The corresponding boundary conditions are a characteristic impedance in the uniform waveguide at the right, $z>L$, and a given plane velocity at $z=0$. The frequency is below the first mode cutoff frequency at the infinite end (f_c in the sequel) in

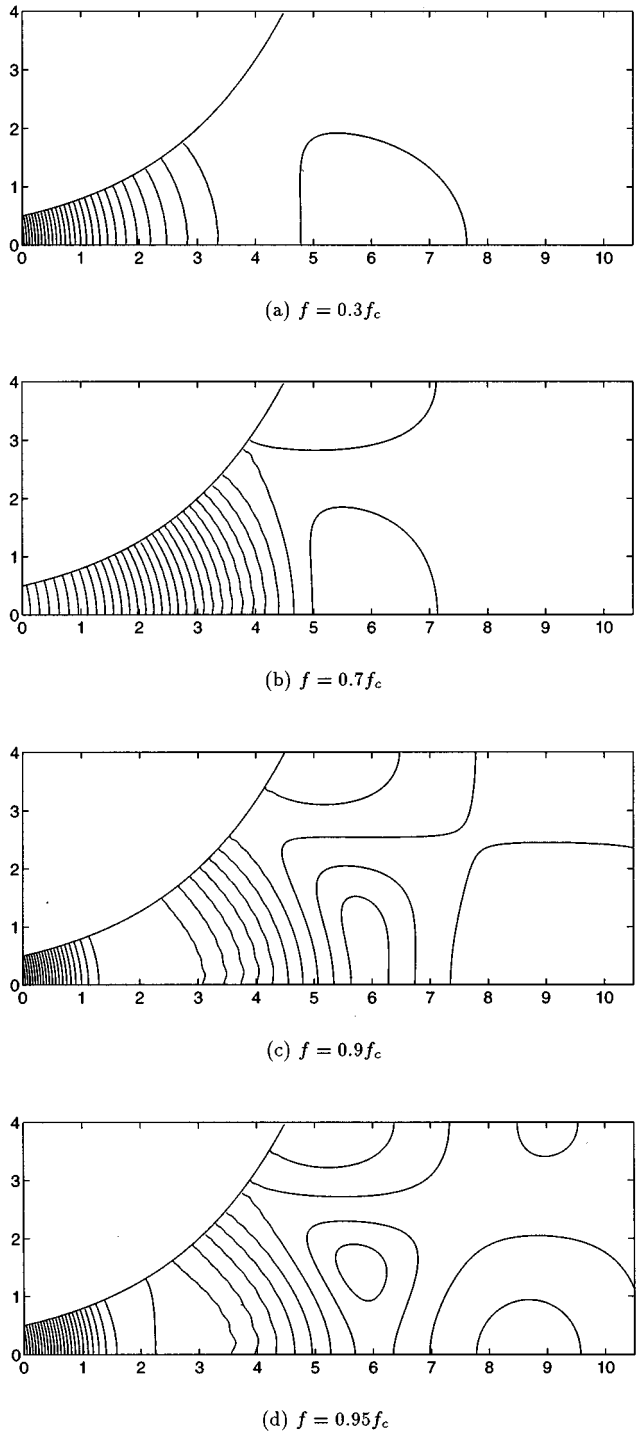

FIG. 4. Modulus of the pressure for four different frequencies.

order that the comparison with the MPW solution will make sense.

The results of the calculations with 15 modes are shown in Fig. 4. It represents the modulus of the pressure, in the exponential horn, for four different frequencies below f_c. The parameters of the geometry are such that $R_f = 8R_0$, $L = 9R_0$, and the typical step size for the integration is $\lambda/100$. Even for frequency as low as $f = 0.3f_c$ the pattern of the isovalues is far from being that of a plane wave, demonstrating the hazardous nature of the MPW equation. It is confirmed that the correct orthogonal boundary condition to the walls are well achieved with our method in spite of the projection on the basic functions (55) (see Sec. I B). This nonplane behavior becomes more and more obvious with increasing frequency as ripples appear due to the finite truncation of the number of modes. Conservation of energy has been checked in each case and was found to be accurate at the order of 0.5%. For a frequency quite close to f_c [Fig. 4(d)], although the second mode remains evanescent, its typical length of influence $(2\pi/k_1)$ diverges and an advantage of our approach is that we do not have to perform the computation with a long termination L (to let mode 1 vanish) since the boundary condition at the right (matrix impedance Z_c) is analytically known in the straight duct.

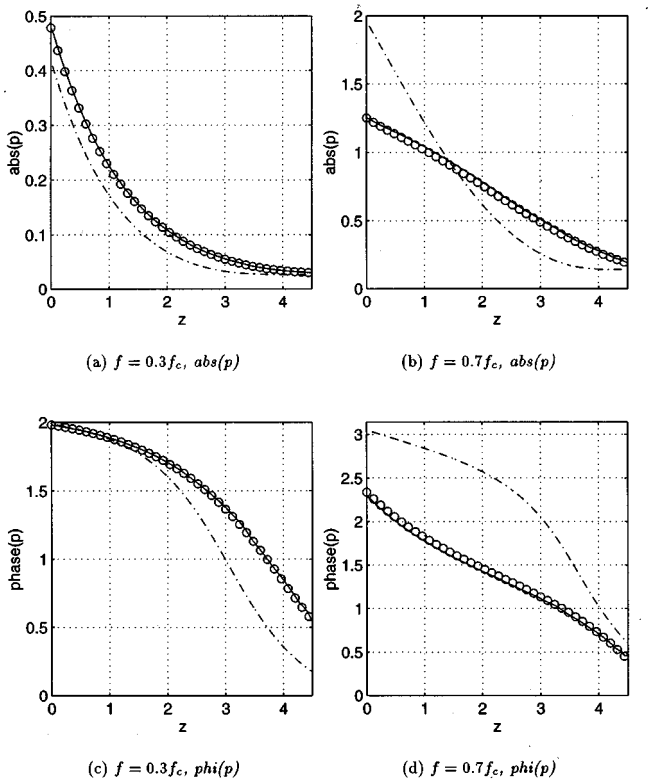

FIG. 5. (a), (b) Modulus and (c), (d) phase of the pressure along the axis ($r = 0$). Ansys (plain), our method (circle, ○), and MPW (dashed, -·-).

To validate our approach, calculations with a finite element method (FEM) code (ANSYS) have been done in the same geometry. The number of nodes was 3600 corresponding to an elementary cell of side $\lambda/20$. The boundary condition at the right was to impose $p = \rho c v_z$ at the termination, which is only an approximation to the perfect infinite termination. The patterns obtained were quite similar and nearly impossible to differentiate from those obtained with the multimodal approach. Figure 5 shows the comparison of the results obtained with the plane-wave approximation, the FEM code, and our method. The two latter methods are almost in perfect agreement for both frequencies ($f = 0.3f_c$ and $f = 0.7f_c$), while the plane-wave approximation (MPW) already shows inaccurate features. It can be concluded that, on

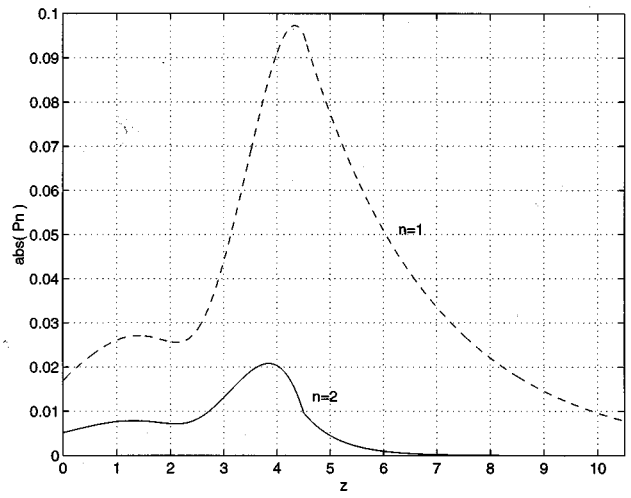

FIG. 6. Modulus of components $P_n(z)$ for the first two nonplane modes, $n=1$ (dotted) and $n=2$ (plain). $f=0.9f_c$.

the one hand, our method is validated by its agreement with the FEM results and, on the other hand, its utility is demonstrated by the inaccuracy of the plane-wave approximation (MPW). Figure 6 shows the evolution of the two first nonplane component of pressure, $P_1(z)$ and $P_2(z)$. We understand why the plane-wave approximation fails to give good results since it can be seen that the other modes cannot be neglected. As mentioned earlier, an interesting property of the exponential horn is that it is considered a high-pass filter. We have performed the calculation of the reflection coefficient (see Appendix D) with our multimodal method and compared it with the classical analytical model of MPW, which is usually used for this range of frequency (see Fig. 7). It appears there are dramatic differences, of about 25%, for the estimated cutoff frequencies in between the two cases. Hence, even when only the plane wave is propagating, a higher-order modal method, as ours, has to be used in order to get the right model for the horn.

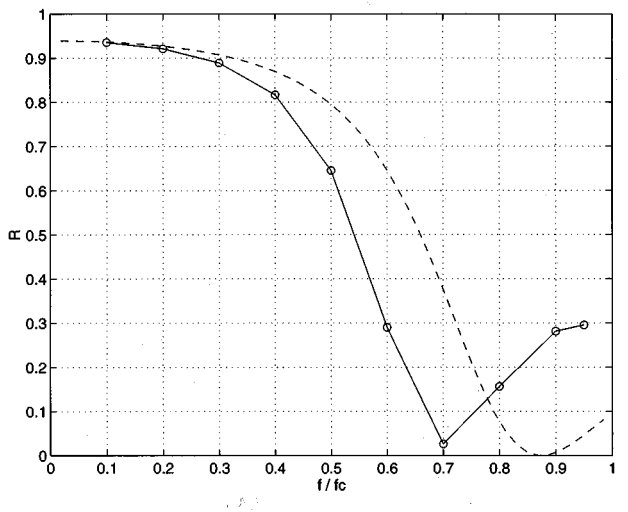

FIG. 7. Reflection coefficient for MPW (dashed, - - -) and our method (circle, ○) against f/f_c.

IV. CONCLUSION

We have presented a multimodal approach to the problem of determining the wave propagation in waveguides with varying cross section. It has been shown that the major potential failure of this projection method, i.e., nonfulfillment of the boundary conditions at a hard wall, has been avoided due to the specific nature of the coupling between the modes. This gives alternative means to the usual FEM or BEM methods that sometimes do not provide a well-posed modelization for the radiation conditions. For instance, our method gives a natural boundary condition for an infinite guide termination, which is simply the characteristic impedance matrix; finding this boundary condition is a much more difficult task without multimodal decomposition. Furthermore, once the impedance matrix has been calculated for a given geometry with a given radiation condition, the field resulting from many different sources can be obtained in a very simple manner.

Results show excellent agreement with FEM code at low frequency (below the first cutoff). It is also shown that even at rather low frequency, evanescent modes have dramatic effects that make our equations much more accurate than the usual matched plane-wave approximation. An example is the cutoff of an exponential horn that is analytically known under the plane-wave assumption but which appears to be inaccurate using this method, and requires higher-order modes to be calculated correctly.

APPENDIX A

In this Appendix a new proof of the matricial horn equation is given. We restrict to axisymmetric case without loss of generality. The idea is that the first-order expansion $F=I-\epsilon Q$ (Ref. 7) for the discontinuity matrix is valid only for each column. Hence, terms such as ${}^tFX$ ($\mathbf{X}$ vector) will be valid in this expansion but not those such as FX because in the latter case the column indices tend to infinity. Starting from Eqs. (12), (13), and (14), in the case of infinitesimal discontinuity, the mth eigenfunction can be expressed at first order as

$$\psi_{2n}=\psi_{1n}+(R_2-R_1)\,\frac{\partial\psi}{\partial R}+O(f(n)(\Delta R)^2), \tag{A1}$$

where $\Delta R=R_2-R_1$ is the difference between the two successive radii. This is valid as long as the index n is kept at a finite value and does not tend to infinity. Then for discontinuity equation (13), taken at a fixed n,

$$U_{2n}=\sum_m F_{mn}U_{1m}, \tag{A2}$$

$$=\frac{1}{S_1}\sum_m\left(\int\int_{S_1}\psi_{1m}\psi_{1n}\,dS+(\Delta R)\int\int_{S_1}\psi_{1m}\times\frac{\partial\psi_{1n}}{\partial R}\,dS+\int\int_{S_1}\psi_{1m}O(f(n)(\Delta R)^2)\,dS\right), \tag{A3}$$

$$= \sum_m \left(\delta_{mn} U_{1m} - \frac{1}{S_1} 2\pi R \Delta R Q_{mn} U_{1m} + O((\Delta R)^2) \right), \tag{A4}$$

$$= U_{1n} - \frac{\Delta S}{S_1} \sum_m Q_{mn} U_{1m} + O((\Delta R)^2), \tag{A5}$$

where $\Delta S = (S_2 - S_1)$ and

$$Q_{mn} = (2\pi R)^{-1} \int \int_{S_1} \psi_{1m} \frac{\partial \psi_{1n}}{\partial R} \, dS.$$

By taking the limit, a discontinuity induces a derivative

$$\mathbf{U}' = -\frac{S'}{S} {}^t Q \mathbf{U}. \tag{A6}$$

For the matched pressure, one cannot deduce an expansion from Eq. (A1) because the discontinuity relation (12), that is, $P_{1n} = \Sigma_m F_{nm} P_{2m}$, has the column index m that tends to infinity. Therefore, instead of Eq. (12), which corresponds to the so-called mixed method,[11] we apply a ''major unilateral method;'' pressure and velocity are both projected on the bigger cross section S_2 of the discontinuity. This gives for the pressure

$$\int \int_{S_2} p_2 \psi_{2n} \, dS = \int \int_{S_1} p_1 \psi_{2n} \, dS + \int \int_{S_2 - S_1} p_2 \psi_{2n} \, dS. \tag{A7}$$

The first term is handled as previously for the velocity. For the second term of the right-hand part, $p_2(r) = p_2(R_1) + O(\Delta R) = p_1(R_1) + O(\Delta R)$ and $\psi_{2n}(r) = \psi_{2n}(R_2) + O(f(n)\Delta R) = 1 + O(f(n)\Delta R)$, hence (always at first order)

$$\int \int_{S_2 - S_1} p_2 \psi_{2n} \, dS = p_1(R_1) \int \int_{S_2 - S_1} dS + O((\Delta R)^2) = \Delta S p_1(R_1) + O((\Delta R)^2). \tag{A8}$$

Equation (64) is reduced to

$$S_2 P_{2n} = S_1 P_{1n} - \Delta S \sum_m Q_{mn} P_{1m} + \Delta S \sum_m P_{1m} \psi_{1m}(R_1) + O((\Delta R)^2), \tag{A9}$$

which implies

$$(S\mathbf{P})' = -S' {}^t Q \mathbf{P} + S' \Theta \mathbf{P}, \tag{A10}$$

or equivalently, since $Q + {}^t Q + I = \Theta$ [see Eq. (28)],

$$\mathbf{P}' = -\frac{S'}{S} Q \mathbf{P}. \tag{A11}$$

APPENDIX B

We want to project the two Euler equations, $\partial v_z / \partial z = -jkp$ and $\partial p / \partial z = -jkv_z + 1/(jk)\Delta_\perp p$, together with the correct boundary condition (17). In the following, we will restrict to the axisymmetric case without loss of generality. Following Stevenson's approach, we use Leibniz's rule for an arbitrary function $\zeta = \zeta(z,r)$:

$$\frac{d}{dz} \left(\int \int_S \zeta \, dS \right) = \int \int_S \frac{\partial \zeta}{\partial z} \, dS + \oint_C \zeta R'(z) \, dC. \tag{B1}$$

It follows that

$$\int \int_S \psi_n \frac{\partial \zeta}{\partial z} \, dS = \frac{d}{dz} \left(\int \int_S \psi_n \zeta \, dS \right) - \int \int_S \zeta \frac{\partial \psi_n}{\partial z} \, dS - \oint_C \zeta \psi_n R'(z) \, dC. \tag{B2}$$

Using this relation and the series decomposition of p and v_z in (4) enables us to get the projection for $\partial p / \partial z$ and $\partial v_z / \partial z$. Using ζ once more as an example, and defining $\zeta = \Sigma_m \zeta_m \psi_m$, (70) becomes

$$\int \int_S \psi_n \frac{\partial \zeta}{\partial z} \, dS = (S\zeta_n)' - \sum_m \left(\int \int_S \psi_m \frac{\partial \psi_n}{\partial z} \, dS \right) \zeta_m - \sum_m \left(\oint_C \psi_m \psi_n R'(z) \, dC \right) \zeta_m. \tag{B3}$$

Applying the same procedure to p and v_z enables us to obtain the projection of the terms of the Euler equations for $\partial p / \partial z, \partial v_z / \partial z$. In matricial form, this gives us

$$\int \int_S \frac{\partial p}{\partial z} \boldsymbol{\psi} \, dS = S' \mathbf{P} + S \mathbf{P}' + S' {}^t Q \mathbf{P} - S' \Theta \mathbf{P} \tag{B4}$$

and

$$\int \int_S \frac{\partial v_z}{\partial z} \boldsymbol{\psi} \, dS = \mathbf{U}' + \frac{S'}{S} {}^t Q \mathbf{U} - \frac{S'}{S} \Theta \mathbf{U}, \tag{B5}$$

where Q is defined in Eq. (40) and $\Theta_{mn} = 1$. The case of $\Delta_\perp p$ is treated differently. Using Green's theorem and the boundary condition for ψ_i (7) and for p (17),

$$\begin{aligned} &\int \int_S \Delta_\perp p \psi_n \, dS \\ &= \int \int_S p \Delta_\perp \psi_n \, dS + \oint_C \left(\psi_n \frac{\partial p}{\partial r} - p \frac{\partial \psi_n}{\partial r} \right) dC \\ &= -\alpha_n^2 \int \int_S p \psi_n \, dS + \oint_C R'(z) \frac{\partial p}{\partial z} \psi_n \, dC \\ &= -\alpha_n^2 S P_n - jk \oint_C R'(z) v_z \psi_n \, dC. \end{aligned}$$

APPENDIX C

To project the Helmholtz equation, $\partial^2 p / \partial z^2 + \Delta_\perp p + k^2 p = 0$ with $\partial p / \partial n = 0$ on the wall, in the same manner, one has to do the same calculation as in Appendix A for the new term $\partial^2 p / \partial z^2$. By applying Leibniz's rule twice, we have

$$\frac{d^2}{dz^2}\left(\int\int_S p\psi_n\, dS\right)$$
$$=\frac{d}{dz}\left(\int\int_S \frac{\partial p\psi_n}{\partial z}\, dS+\oint_C p\psi_n R'(z)\, dC\right)$$
$$=\int\int_S \frac{\partial^2 p\psi_n}{\partial z^2}\, dS+\oint_C \frac{\partial p\psi_n}{\partial z} R'(z)\, dC$$
$$+\frac{d}{dz}\left(\oint_C p\psi_n R'(z)\, dC\right). \tag{C1}$$

The third term can be handled as follows: The derivative d/dz has to be taken along the wall and is equal to $\partial/\partial z+R'(z)\partial/\partial r$. But we know the boundary condition (17) implies that $\partial/\partial r-R'(z)\partial/\partial z=0$ at the wall. This gives $d/dz=(1+R'(z)^2)\partial/\partial z$. So, recalling that $\psi_n(R,z)=1$, the third term becomes

$$\frac{d}{dz}\left(S'(z)p(R(z),z)\right)$$
$$=S''(z)p(R,z)+(1+R'(z)^2)\frac{\partial p}{\partial z}(R)$$
$$=S''(z)p(R,z)-jkS'(1+R'(z)^2)v_z(R,z). \tag{C2}$$

Finally, we have:

$$\int\int_S \frac{\partial^2 p}{\partial z^2}\psi_n\, dS$$
$$=\frac{d^2}{dz^2}\left(\int\int_S p\psi_n\, dS\right)-\int\int_S p\frac{\partial^2\psi_n}{\partial z^2}\, dS$$
$$+2jk\int\int_S v_z\frac{\partial\psi_n}{\partial z}\, dS+jk\oint_C \psi_n v_z R'(z)\, dC$$
$$+S''(z)p(R,z)-jkS'(1+R'(z)^2)v_z(R,z). \tag{C3}$$

Equation (76) can now be projected on the ψ_m basis:

$$\int\int_S \frac{\partial^2 p}{\partial z^2}\psi_n\, dS$$
$$=\frac{d^2}{dz^2}(SP_n)-\sum_m \int\int_S \psi m\frac{\partial^2\psi_n}{\partial z^2}\, dSP_m$$
$$+2\sum_m \frac{jk}{S}\int\int_S \psi_m\frac{\partial\psi_n}{\partial z}\, dSU_m+\sum_m \frac{jk}{S}$$
$$\times\oint_C \psi_n\psi_m R'(z)\, dCU_m-\sum_m S''(z)\psi_m(R)P_m$$
$$+\sum_m \frac{jkS'}{S}(1+R'(z)^2)\psi_m(R)U_m, \tag{C4}$$

which in matricial form becomes

$$\int\int_S \frac{\partial^2 p}{\partial z^2}\boldsymbol{\psi}\, dS$$
$$=S\mathbf{P}''+2S'\mathbf{P}'+S''\mathbf{P}-T\mathbf{P}-2\frac{jkS'}{S}{}^tQ\mathbf{U}+\frac{jkS'}{S}\Theta\mathbf{U}$$
$$-S''(z)\Theta\mathbf{P}+\frac{jkS'}{S}(1+R'(z)^2)\Theta\mathbf{U}. \tag{C5}$$

This has now been obtained without having performed any derivation of infinite series.

APPENDIX D

Decomposing the pressure and the velocity in an uniform waveguide as the sum of incident and reflected parts, we have

$$\mathbf{P}=\mathbf{P}_+ +\mathbf{P}_- =Z_c(\mathbf{U}_+ -\mathbf{U}_-), \tag{D1}$$
$$\mathbf{U}=\mathbf{U}_+ +\mathbf{U}_-, \tag{D2}$$

where Z_c is the characteristic impedance matrix at this abscissa. If we know the impedance $Z_1(\mathbf{P}=Z_1\mathbf{U})$, it follows that

$$\mathbf{U}_-=(Z_1+Z_c)^{-1}(Z_c-Z_1)\mathbf{U}_+. \tag{D3}$$

Then for the energy flux

$$W_1=\mathrm{Re}\{{}^t\mathbf{P}\cdot\mathbf{U}^*\},$$
$$=\mathrm{Re}\{{}^t\mathbf{P}_+\cdot\mathbf{U}_+^*\}+\mathrm{Re}\{{}^t\mathbf{P}_-\cdot\mathbf{U}_-^*\}$$
$$+\mathrm{Re}\{{}^t\mathbf{P}_+\cdot\mathbf{U}_-^*+{}^t\mathbf{P}_-\cdot\mathbf{U}_+^*\},$$
$$=\mathrm{Re}\{{}^t\mathbf{U}_+Z_c\mathbf{U}_+^*-{}^t\mathbf{U}_-Z_c\mathbf{U}_-^*\}$$
$$-2\,\mathrm{Im}\{Z_c\}\sum_m \mathrm{Im}\{U_{+,m}U_{-,m}\}, \tag{D4}$$

where m denotes the m'th element in the appropriate vector.

If the $\mathbf{U}_+$ have no components on the evanescents modes, we get a decomposition for the flux W_1 in incident (W_{1+}) and reflected (W_{1-}) parts:

$$W_1=\mathrm{Re}\{{}^t\mathbf{U}_+Z_c\mathbf{U}_+^*-{}^t\mathbf{U}_-Z_c\mathbf{U}_-^*\}=W_{1+}-W_{1-}. \tag{D5}$$

Defining the reflection coefficient R, and the transmission coefficient T as

$$R=\frac{W_{1-}}{W_{1+}},\quad T=\frac{W_1}{W_{1+}},$$

the usual relation, $R+T=1$, is recovered. For our computation U_+ was chosen as the plane mode, i.e., $U_+=(1,0,0,...,0)$. Nevertheless, it should be noticed that any vector U_+ with zero component for the evanescent modes could have been chosen.

APPENDIX E

By assuming the plane-wave approximation in a waveguide with nonuniform section $S(z)$ it is easy to get the evolution of both pressure p and axial velocity v_z:

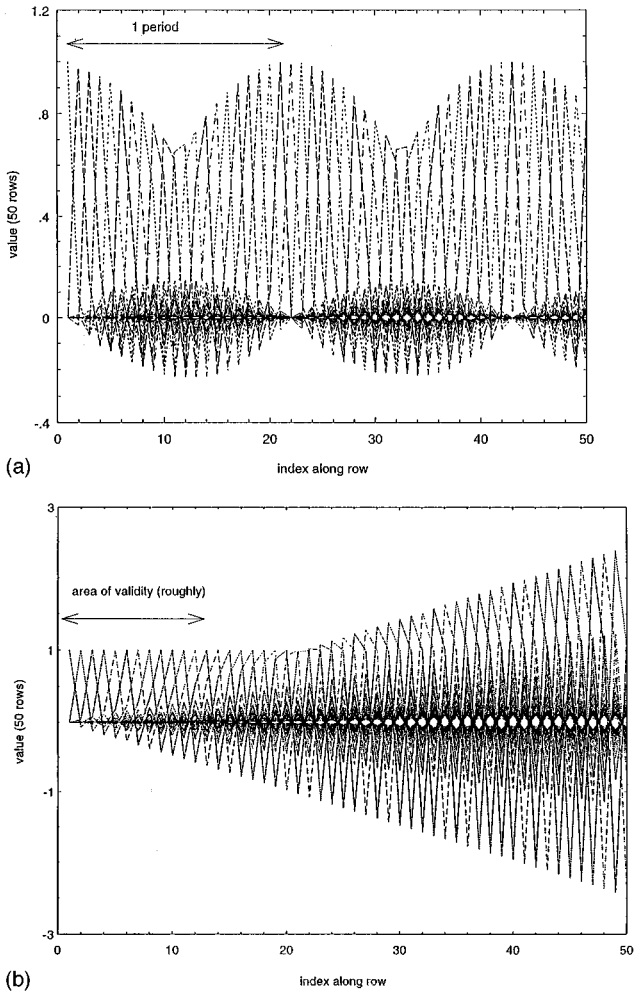

FIG. F1. Plot superimposing the rows of (a) F and (b) $I-\epsilon Q$.

$$p' = -jkv_z,$$
$$v_z' = -jkp - \frac{S'}{S} v_z. \tag{E1}$$

Eliminating v_z yields the second-order MPW differential equation for the pressure:

$$p'' + \frac{S'}{S} p' + k^2 p = 0. \tag{E2}$$

For an exponential horn with a radius R so that $R = R_0 e^{m(z-z_0)}$, the solutions are; for the pressure

$$p = e^{-mz}(Ae^{-jaz} + Be^{jaz}), \tag{E3}$$

and for the longitudinal velocity

$$v_z = \frac{j}{k} e^{-mz}(-(m+ja)Ae^{-jaz} + (ja-m)Be^{jaz}), \tag{E4}$$

where the wave number a is a solution of $a^2 = k^2 - m^2$. When the frequencies are low enough so that $k < m$, there is no propagating modes. This is the well-known high-pass filter of the exponential horn.

If now we define the impedance as $\chi = p/v_z$, its evolution is governed by the Riccati equation

$$\chi' = -jk(1-\chi^2) + 2m\chi. \tag{E5}$$

The general solution is found to be

$$\chi = \frac{a\chi_0 - (k + jm\chi_0)\tanh(ja(z-z_0))}{a - (k\chi_0 - jm)\tanh(ja(z-z_0))} \tag{E6}$$

if the impedance at $z = z_0$ is χ_0.

APPENDIX F

In this Appendix we examine some properties of the linear approximation of the F matrix, $F_{\text{app}} = I - \epsilon Q$. In a case such as ours, where F is infinite, such an approximation should be treated with care. When obtaining Eqs. (26) and (27) using the IDS method, it appears *a priori* that for any epsilon, defined as $\epsilon = (S_2 - S_1)/S_1$, the above approximation should fail to sufficiently high indices in F. As we have shown in Appendix A, this approximation remains valid for the IDS method, due to the fact that we use the linear approximation along columns of F only.

On the other hand, if we wish to use the above approximation in implementing the DS method, to obviate the lengthy calculation of the exact F matrix we will discover a direct relationship between ϵ and the number modes we can use. We demonstrate how it is determined empirically in the case of bidimendional geometry. The approximation of F, defined as F, for a case where $\epsilon = 1/20$, and for dimensions 50×50, is plotted in Fig. F1(a); the lines of this matrix are plotted one on top of the other on the same axes. In Fig. F1(b) we plot the exact values of F. We see that the envelope of each line of (b) is periodic, with a period of about $2/d\epsilon$, whereas the envelope of (a) increases steadily. Thus, the approximation becomes steadily worse as the index of the line in F increases. A reasonable limit for the number of lines is $2/3d\epsilon$, or about one-third of the period of the envelope in Fig. F1(b). This is equivalent to limiting the number of modes to the same value. Note that this limit is empirical, in the sense that there is not a sudden degradation in accuracy if it is exceeded slightly. Once the number of modes exceeds $1/d\epsilon$, though, the difference between F and F clearly grows dramatically.

APPENDIX G

Applying the general results in this paper to the axisymmetric geometry necessitated computation of a number of integrals involving Bessel functions. Since an exhaustive search on our part did not turn up solutions to these integrals in the literature, we present in this appendix these integrals and their analytic solutions, which have been verified as far as possible by computer. Denoting γ_i as a zero of $J_1(t)$, we obtained the following:

$$\int_0^1 t^2 J_0(\gamma_m t) J_1(\gamma_n t)\, dt$$
$$= \begin{cases} -J_0(\gamma_m) J_0(\gamma_n) \dfrac{\gamma_n}{\gamma_n^2 - \gamma_m^2}, & m \neq n, \\ 0 \quad m = n, \end{cases} \tag{G1}$$

$$\int_0^1 t^3 J_0(\gamma_m t) J_0(\gamma_n t)\, dt$$

$$= \begin{cases} 2J_0(\gamma_m) J_0(\gamma_n)\, \dfrac{\gamma_n^2+\gamma_m^2}{(\gamma_n^2-\gamma_m^2)^2}, & m \neq n, \\ \frac{1}{6} J_0^2(\gamma_m), & m = n, \end{cases} \tag{G2}$$

$$\int_0^1 t^3 J_1(\gamma_m t) J_1(\gamma_n t)\, dt$$

$$= \begin{cases} 2J_0(\gamma_m) J_0(\gamma_n)\, \dfrac{\gamma_n^4+\gamma_m^4}{\gamma_m \gamma_n (\gamma_n^2-\gamma_m^2)^2}, & m \neq m, \\ \frac{1}{6} J_0^2(\gamma_m), & m = n, \end{cases} \tag{G3}$$

$$\int_0^1 t^2 J_1(\gamma_n t)\, dt = -\frac{J_0(\gamma_n)}{\gamma_n}, \tag{G4}$$

$$\int_0^1 t^3 J_0(\gamma_n t)\, dt = 2\frac{J_0(\gamma_n)}{\gamma_n^2}. \tag{G5}$$

APPENDIX H

Using the identities of Appendix F enables us to obtain the expression of matrix T in the axisymmetric case:

$$T_{ij} = -2\pi((R''R - R'^2) Q_{ji} + R'^2 X_{ij}), \tag{H1}$$

where matrix X is

$$X_{ij} = \begin{cases} 2\gamma_i^2\, \dfrac{\gamma_i^2+\gamma_j^2}{(\gamma_i^2-\gamma_j^2)^2}, & i \neq j, \\ \frac{1}{6}\gamma_i^2, & i = j. \end{cases} \tag{H2}$$

[1] L. M. B. C. Campos, ''Some general properties of the exact acoustic fields in horns and baffles,'' J. Sound Vib. **95**(2), 177–201 (1984).

[2] E. Eisner, ''Complete solution of the Webster horn equation,'' J. Audio. Eng. Soc. **41**, 1126–1146 (1967).

[3] G. R. Putland, ''Every one-parameter acoustic field obeys Webster's horn equation,'' J. Audio Eng. Soc. **41**(6), 435–451 (1993).

[4] A. F. Stevenson, ''Exact and approximate equations for wave propagation in acoustic horns,'' J. Appl. Phys. **22**(12), 1461–1463 (1951).

[5] R. J. Alfredson, ''The propagation of sound in a circular duct of continuously varying cross-sectional area,'' J. Sound Vib. **23**(4), 433–442 (1972).

[6] A. Roure, Propagation Guidee, Etude des Discontinuites, Doctoral thesis, Universite of Aix-Marseille, 1976.

[7] J. Kergomard, ''Une equation matricielle des pavillons acoustiques,'' C. R. Acad. Sci. Paris Ser. II **316**, 1691–1694 (1993).

[8] M. Razavy, ''Localized and propagating modes in acoustical waveguides with variable cross section,'' J. Acoust. Soc. Am. **95**, 2371–2377.

[9] P. Morse and U. Ingard, *Theoretical Acoustics* (McGraw-Hill, New York, 1952).

[10] J. Kergomard, ''Calculation of discontinuities in waveguides using mode-matching method: An alternative to the scattering matrix approach,'' J. Acoustique **4**, 111–137, (1991).

[11] C. Vassallo, *Theorie des Guides d'Ondes Electromagnetiques* (Eyrolles, Paris, 1985), Vol. II, p. 583.

[12] W. E. Zorumski, ''Generalized radiation impedances and reflection coefficients of circular and annular ducts,'' J. Acoust. Soc. Am. **54**, 1667–1673 (1973).

[13] W. H. Press, W. T. Vetterling, S. A. Teukolsky, and B. P. Flannery, *Numerical Recipes* (Cambridge U. P., London, 1992).

[14] S. R. Rutherford and K. E. Hawker, ''Consistent coupled mode theory of sound propagation for a class of nonseparable problems,'' J. Acoust. Soc. Am. **70**, 554–564 (1981).

[15] J. Kergomard, A. Garcia, G. Tagui, and J. P. Dalmont, ''Analysis of higher order mode effects in an expansion chamber using modal theory and equivalent electrical circuits,'' J. Sound Vib. **129**(3), 457–475 (1989).

[16] V. Pagneux, J. Kergomard, and G. Marquette, *Propagation multimodale en géométrie complexe*, Lille, Congrès Français de Mecanique (A.U.M., Paris, 1993), pp. 1045–1049.

[17] A. M. Bruneau, M. Bruneau, Ph. Herzog, and J. Kergomard, ''Boundary layer attenuation of higher order modes in waveguides,'' J. Sound Vib. **119**(1), 15–27 (1987).

[18] N. Amir, V. Pagneux, and J. Kergomard, ''A study of wave propagation in varying cross-section waveguides by model decomposition. Part II. Results,'' J. Acoust. Soc. Am. (submitted).

[19] S. A. Schelkunoff, ''Conversion of Maxwell's equations into generalized telegraphist's equations,'' Bell Syst. Tech. J. **34**, 995–1043 (1955).